

# Supporting information for “The impact of molecular self-organisation on the atmospheric fate of a cooking aerosol proxy”.

Adam Milsom<sup>1</sup>, Adam M. Squires<sup>2</sup>, Andrew D. Ward<sup>3</sup> and Christian Pfrang<sup>1,4</sup>.

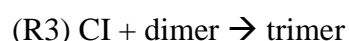
<sup>1</sup>University of Birmingham, School of Geography, Earth and Environmental Sciences, Edgbaston, Birmingham, UK

<sup>2</sup>University of Bath, Department of Chemistry, South Building, Soldier Down Ln, Claverton Down, Bath, UK

<sup>3</sup>Central Laser Facility, STFC Rutherford Appleton Laboratory, Didcot OX11 0FA, UK

<sup>4</sup>Department of Meteorology, University of Reading, Whiteknights, Earley Gate, Reading, UK

## S1. Model reaction scheme



A simplified form of the reaction scheme used by Hosny *et al.* has been used (Hosny *et al.*, 2016). The initial reaction of oleic acid with ozone ( $\text{O}_3$ ) forms nonanal (NN) or a 9-carbon ( $\text{C}_9$ ) product (nonanoic acid, 9-oxononanoic acid or azelaic acid) plus a Criegee intermediate (CI). The relative amount of NN and  $\text{C}_9$  products is determined by the branching ratio ( $c$ ). We have also included the loss of NN from the surface due to its high volatility. The CI then goes onto react with a  $\text{C}_9$  product to form the dimer. This dimer then reacts with another CI to form the trimer, which represents all higher order products in this model scheme.

Since this is a simplified reaction scheme and we assume that diffusion parameters dominate the reaction kinetics, we have held all reaction rates to those optimised by Hosny *et al.* (Hosny *et al.*, 2016) (see next section).

## S2. Model parameters

| <i>Parameter</i> | <i>Description</i>                                             | <i>Value</i>             | <i>Units</i>                    |
|------------------|----------------------------------------------------------------|--------------------------|---------------------------------|
| $k_{BR,1}$       | Bulk reaction rate coefficient for R1                          | $1.13 \times 10^{-18}$   | $\text{cm}^3 \text{s}^{-1}$     |
| $k_{BR,2}$       | Bulk reaction rate coefficient for R2                          | $1.86 \times 10^{-17}$   | $\text{cm}^3 \text{s}^{-1}$     |
| $k_{BR,3}$       | Bulk reaction rate coefficient for R3                          | $1.99 \times 10^{-16}$   | $\text{cm}^3 \text{s}^{-1}$     |
| $c$              | Stoichiometric coefficient (branching ratio)                   | 0.454                    |                                 |
| $H_{cp,O3}$      | Henry's law coefficient of O3 in organics                      | $6.66 \times 10^{-4}$    | $\text{mol cm}^{-1} \text{atm}$ |
| $T_{d,O3}$       | Surface desorption lifetime of O3                              | $1.67 \times 10^{-7}$    | s                               |
| $\alpha_{s,0}$   | Surface accommodation coefficient of O3                        | 0.13                     |                                 |
| $D_{dimer}$      | Bulk diffusion coefficient of the dimer                        | $[1.03 \times 10^{-12}]$ | $\text{cm}^2 \text{s}^{-1}$     |
| $f_{diff}$       | Power law scaling factor for oligomer viscosity                | 3.96                     |                                 |
| $D_{X,lam}$      | Bulk diffusion coefficient of ozone in the lamellar phase      | $[3.35 \times 10^{-12}]$ | $\text{cm}^2 \text{s}^{-1}$     |
| $D_{Y,lam}$      | Bulk diffusion coefficient of oleic acid in the lamellar phase | $[2.81 \times 10^{-12}]$ | $\text{cm}^2 \text{s}^{-1}$     |
| $D_{X,di}$       | Bulk diffusion coefficient of O3 in the dimer                  | $[4.66 \times 10^{-9}]$  | $\text{cm}^2 \text{s}^{-1}$     |
| $D_{Y,di}$       | Bulk diffusion coefficient of oleic acid in the dimer          | $[8.85 \times 10^{-11}]$ | $\text{cm}^2 \text{s}^{-1}$     |
| $D_{X,tri}$      | Bulk diffusion coefficient of O3 in the trimer                 | $[1.49 \times 10^{-12}]$ | $\text{cm}^2 \text{s}^{-1}$     |
| $D_{y,tri}$      | Bulk diffusion coefficient of oleic acid in the trimer         | $[8.16 \times 10^{-11}]$ | $\text{cm}^2 \text{s}^{-1}$     |
| $f_{slr}$        | Scaling factor for surface reaction rates                      | $4.41 \times 10^{-6}$    | $\text{cm}^{-1}$                |
| $k_{loss,NN}$    | Rate of nonanal loss from particle surface                     | 1.4                      | $\text{s}^{-1}$                 |

Table S1. Parameters used in the model. Parameters in square brackets were optimised using the differential evolution global optimisation algorithm.

All unvaried parameters are constrained to the values reported by Hosny *et al.* (Hosny *et al.*, 2016) except for the rate of nonanal loss from the particle surface ( $k_{loss,NN}$ ), which was found not to affect the model output under these conditions and set to a value of  $1.4 \text{ s}^{-1}$ .

|                    | <i>Film thickness / <math>\mu\text{m}</math></i> |                        |                        |                        |
|--------------------|--------------------------------------------------|------------------------|------------------------|------------------------|
|                    | <i>0.59</i>                                      | <i>0.91</i>            | <i>0.98</i>            | <i>1.66</i>            |
| $D_{x,\text{lam}}$ | $4.58 \times 10^{-12}$                           | $1.13 \times 10^{-12}$ | $8.78 \times 10^{-10}$ | $5.64 \times 10^{-12}$ |
| $D_{x,\text{tri}}$ | $5.64 \times 10^{-10}$                           | $3.42 \times 10^{-9}$  | $9.76 \times 10^{-9}$  | $9.12 \times 10^{-9}$  |
| $D_{y,\text{lam}}$ | $8.45 \times 10^{-13}$                           | $1.08 \times 10^{-12}$ | $7.32 \times 10^{-13}$ | $5.54 \times 10^{-12}$ |
| $D_{y,\text{tri}}$ | $1.24 \times 10^{-11}$                           | $1.33 \times 10^{-11}$ | $9.88 \times 10^{-11}$ | $4.89 \times 10^{-11}$ |
| $D_{\text{di}}$    | $4.20 \times 10^{-10}$                           | $9.49 \times 10^{-10}$ | $6.33 \times 10^{-10}$ | $6.28 \times 10^{-10}$ |
| $D_{x,\text{di}}$  | $7.34 \times 10^{-9}$                            | $2.14 \times 10^{-9}$  | $3.86 \times 10^{-9}$  | $7.75 \times 10^{-9}$  |
| $D_{y,\text{di}}$  | $7.92 \times 10^{-11}$                           | $5.03 \times 10^{-11}$ | $9.93 \times 10^{-11}$ | $8.85 \times 10^{-11}$ |

Table S2. Diffusion parameters optimised for individual fits to each separate experimental decay data presented in Fig. 1 of the main text. All values are in units of  $\text{cm}^2 \text{s}^{-1}$ .

### S3. Film composition evolution for liquid oleic acid model run

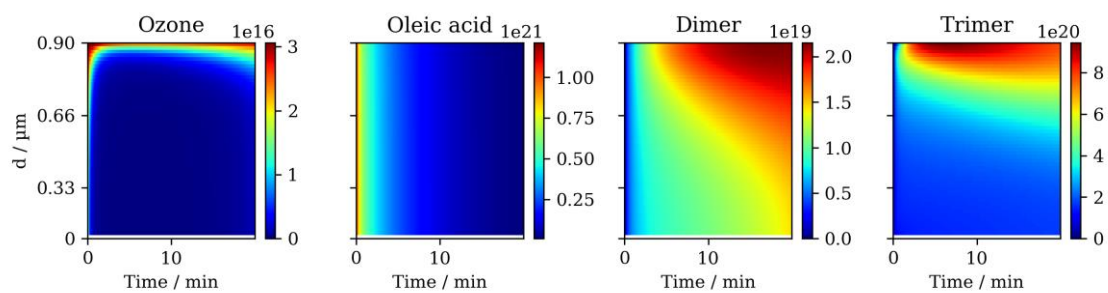
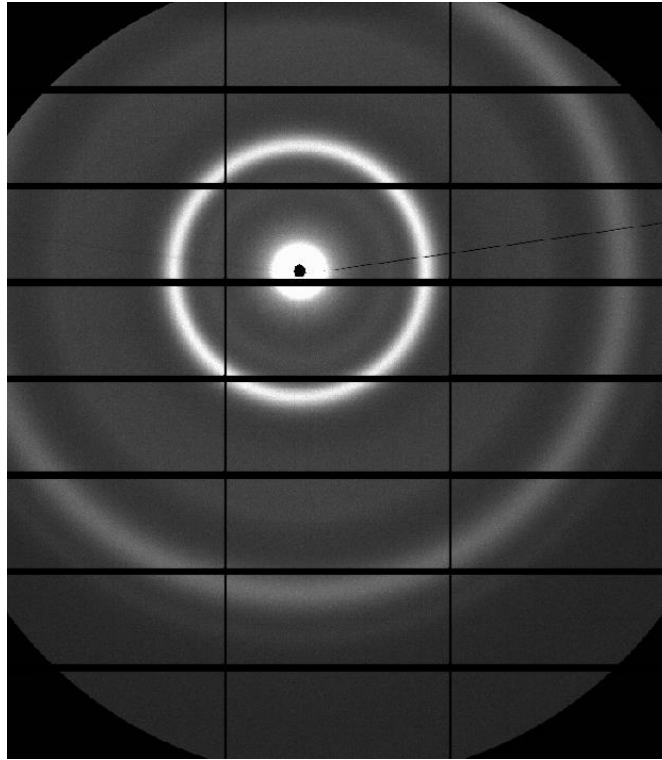


Figure S1. Evolution of component concentration for model runs using liquid oleic acid diffusivity parameters described in the main text. d: distance from the film core.  $[\text{O}_3] = 77$  ppm. Concentrations are in  $\text{cm}^{-3}$ .

#### S4. 2-D SAXS pattern of a coated capillary



*Figure S1. 2-D SAXS pattern of a capillary coated with the oleic acid-sodium oleate (1:1 wt) proxy, showing diffuse scattering rings. The outer ring arises from the Kapton detector window.*

The 2-D scattering pattern from the experiment used in this modelling study exhibits diffuse scattering rings with an even intensity (see the most intense scattering ring in Fig. S2) (Milsom et al., 2021). There are no regions of increased scattered intensity around each scattering ring, therefore the lamellae in are randomly oriented. Lamellar phase orientation would result in either a “spotty” scattering ring or a scattering ring where only certain opposing arcs are visible.

## References

Hosny, N. A., Fitzgerald, C., Vyšniauskas, A., Athanasiadis, A., Berkemeier, T., Uygur, N., Pöschl, U., Shiraiwa, M., Kalberer, M., Pope, F. D. and Kuimova, M. K.: Direct imaging of changes in aerosol particle viscosity upon hydration and chemical aging, *Chem. Sci.*, 7(2), 1357–1367, doi:10.1039/c5sc02959g, 2016.

Milsom, A., Squires, A. M., Woden, B., Terrill, N. J., Ward, A. D. and Pfrang, C.: The persistence of a proxy for cooking emissions in megacities: a kinetic study of the ozonolysis of self-assembled films by simultaneous small and wide angle X-ray scattering (SAXS/WAXS) and Raman microscopy, *Faraday Discuss.*, 226, 364–381, doi:10.1039/D0FD00088D, 2021.